Numerical simulation of the laminar-turbulent boundary-layer transition on a hypersonic forebody using the quasi-gas dynamic equations

Ivan A. Shirokov, Tatiana G. Elizarova**, Ivan Fedioun***, Jean-Claude Lengrand****
** Laboratory of Mathematical Modeling in Physics, Moscow State University*
Leninskie Gory, Moscow, 119991 Moscow, Russia
*** Institute of Applied Mathematics, Russian Academy of Sciences*
Miusskaya Sq. 4, 125047 Moscow, Russia
**** Institut de Combustion, Aérothermique, Réactivité, Environnement,*
Centre National de la Recherche Scientifique
1C avenue de la recherche scientifique, 45071 Orléans Cedex 2, France

Abstract
The non-stationary flow along the forebody of a hypersonic vehicle is studied using a numerical simulation based on Quasi-Gas Dynamic (QGD) equations. The frequency spectrum of oscillations occurring during the laminar-turbulent transition is analysed. The main frequencies of computed oscillations correspond to data obtained by a modal linear stability analysis of the given flow. The 3D computations were carried out on a massively parallel computer.

1. Introduction

The prediction of the laminar/turbulent transition in hypersonic flows has a particular interest in the design of hypersonic air-breathing scramjet-powered vehicles. A crucial issue is the design of a well-adapted air inlet, and this is related to the state of the boundary layer (BL) developing on the forebody before being swallowed by the engine. As evidenced both by wind-tunnel experiments and theoretical studies, boundary layer (BL) transition induces oscillations evolving toward turbulence [1, 2]. From an engineering point of view, predicting laminar-turbulent transition is still a challenging task. Current predictive tools rely mostly on the classical, semi-empirical e^N method. However it would be of interest to simulate directly the occurrence and development of flow oscillations.
This is the objective of the present work, based on the so-called Quasi-Gas Dynamic (QGD) equations, developed by Chetverushkin, Elizarova and co-workers [3-5]. QGD equations are identical to Navier-Stokes (NS) equations, except for additional dissipative terms, that are all in factor of a time parameter τ. Depending on the definition taken for τ, these equations can be used in different areas:

1. In rarefied flows, kinetic considerations allow relating τ to the mean intermolecular collision time and the differences with NS equations come from a different approximation of the molecular velocity distribution function.
2. QGD equations can also be obtained by averaging gas dynamics equations over a small time interval, which results in additional smoothing or regularization. The additional terms that appear due to averaging are second-order space derivatives in factor of a small parameter τ that has the dimension of a time. The τ-terms bring an additional entropy production and have a dissipative character. For slowly-variable laminar flows, they have the order $O(\tau^2)$ and influence only the accuracy of the numerical solution. However, for rapidly-variable flows, they have the order $O(\tau)$ and can bring a significant contribution to the solution. This is what happens in turbulent flows and this property is used in the present work.
3. Additional terms can also be regarded as regularization terms, without any physical meaning. They contribute to the stability of the numerical solution. In this case τ relates to grid size and time step. This variant can be used, e.g., for solving Euler equations [4, 5] or in combination with the previously mentioned application to rarefied flows.

In the present work, we relate the value of the averaging parameter τ to the space-grid step h as $\tau \sim h/c$, where c is the local sound velocity, and we interpret the associated viscosity as an original variant of sub-grid dissipation in

Copyright © 2011 by Shirokov I.A. et al.. Published by the EUCASS association with permission.

LES models, that smoothes or averages the fluctuations of flow parameters on a time-space scale depending on discretization. The sub-grid dissipation in QGD equations differs from the turbulent Smagorinsky viscosity, as the τ-terms have another mathematical structure and additional terms appear not only in the momentum and energy equation, but also in the continuity equation. This latter property models the turbulent mass-diffusion, which is inherent to turbulent mixing. Along a wall, the τ-terms vanish. Laminar/turbulent transition is detected through the unsteady character of the numerical solution.
QGD equations have been used successfully to reproduce the oscillating supersonic flow around a spiked-body [3], the flow close to a hollow cylinder [3, 5, 6] or a cavity [3], and the Karman street downstream a cylinder [4]. Laminar-turbulent transition was obtained for the gas flow downstream a backward facing step [4, 7, 8]: as the flow velocity increases, a bifurcation of the solution occurs and the laminar steady flow turns into an unsteady then turbulent regime. The properties of the QGD equations reveal broad capabilities and open perspectives for the simulation of turbulent flows.
As for practical applications, the QGD system of equations allows designing efficient algorithms for computing liquid and gas flows. These algorithms involve conditionally stable schemes where all space-derivatives, including those appearing in convective terms, are approximated by centered finite differences. The regularization τ-terms ensure the stability of the algorithms. The advantages of these algorithms are their simplicity, the facility of their parallelization and their efficiency when applied to unsteady flows.

2 Mathematical formulation and its application

2.1 Previous work

Using the Fluent software, Orlik, Ferrier et al. [1, 2] have computed the steady laminar 3D flowfield around a hypersonic vehicle forebody, with fully variable thermodynamic and transport properties. Then they applied a linear stability analysis for a number of flow conditions. Here we consider only the flow conditions characterized by a Mach number of 6 at an altitude of 25 km. The angle of attack is 4°, resulting in the leeward side being almost parallel to the freestream, and the windward side of interest being inclined by 8° with respect to it. The wall is assumed to be adiabatic. Two contra-rotative vortices are found in the steady laminar solution. The stability analysis indicates $f = 10$ kHz as the most unstable frequency over the whole length of the body. In Fig. 1 the forebody is represented lying on its back to make the windward side visible.

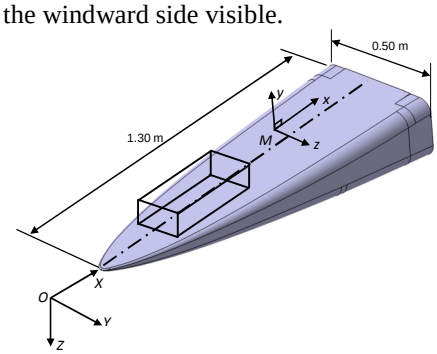

Figure 1: View of the vehicle (upside down)

In the present work, a part of the laminar flowfield, limited to a 3D rectangular domain, adjacent to the wall as shown in Fig.1, has been extracted and used as initial conditions for an unsteady computation based on QGD equations in a 3D formulation.

2.2 Equations

The flow along the vehicle is characterized by its density $\rho(x,y,z,t)$, velocity components $u_x(x,y,z,t)$, $u_y(x,y,z,t)$, $u_z(x,y,z,t)$ and pressure $p(x,y,z,t)$ depending on space and time. The x-direction is the projection of the freestream direction onto the wall. The temperature results from the equation-of-state of the ideal gas:

$$p = \rho RT \tag{1}$$

where $R = \mathcal{R} / \mathcal{M}$ is the gas-constant per unit-mass, $\mathcal{R}$ and $\mathcal{M}$ the universal gas constant and molar mass, respectively. The total energy per unit volume is $E = \rho u^2 / 2 + p / (\gamma - 1)$ and the enthalpy per unit-mass is $H = (E + p) / \rho$, where γ is the specific heat ratio.

Gas dynamics is described by the QGD equations [4, 5] in Cartesian form, using Einstein's convention

$$\frac{\partial}{\partial t}\rho + \nabla_i j_m^i = 0 \tag{2}$$

$$\frac{\partial}{\partial t}\rho u^j + \nabla_i \left(j_m^i u^j \right) + \nabla^j p = \nabla_i \Pi^{ij} \tag{3}$$

$$\frac{\partial}{\partial t}E + \nabla_i \left(j_m^i H \right) + \nabla_i q^i = \nabla_i \left(\Pi^{ij} u_j \right) \tag{4}$$

$$j_m^i = \rho(u^i - w^i), \quad w^i = \frac{\tau}{\rho}\left(\nabla_j \rho u^i u^j + \nabla^i p \right). \tag{5}$$

Expressions for the shear-stress tensor Π^{ij} and the heat flux q^i write

$$\Pi^{ij} = \Pi_{NS}^{ij} + \tau u_i \rho \left(u_k \nabla^k u_j + (\nabla_j p) / \rho \right) + \tau \delta^{ij} \left(u_k \nabla^k p + \gamma p \nabla^k u_k \right) \tag{6}$$

$$\Pi_{NS}^{ij} = \mu \left(\nabla^i u^j + \nabla^j u^i - (2/3)\nabla^k u_k \right) + \varsigma \delta^{ij} \nabla^k u_k \tag{7}$$

$$q^i = q_{NS}^i - \tau u_i \rho \left(u_j \nabla^j \varepsilon + p u_j \nabla^j (1/\rho) \right), \quad q_{NS}^i = -\kappa \nabla^i T, \tag{8}$$

where δ^{ij} is the Kronecker symbol, $\varepsilon = p / \left(\rho (\gamma - 1) \right)$ is the internal energy per unit-mass. The viscosity coefficient μ is taken as a function of temperature:

$$\mu = \mu^0 \times \left(T / T^0 \right)^{\omega}. \tag{9}$$

The coefficient ω is related to the intermolecular potential, μ^0 is a known viscosity at temperature T^0. The heat conductivity is given by

$$\kappa = \left(\mu \gamma R \right) / \left[\mathrm{Pr}\, (\gamma - 1) \right] \tag{10}$$

In the present work, we set $R = 287.048$ J/(kg.K), $\gamma = 1.402$, $\omega = 0.627$, $\mu^0 = 1.477 \times 10^{-5}$ kg/(m.s), $T^0 = 221.6$K and Pr = 0.72 [2]. The bulk viscosity coefficient is given by

$$\varsigma = \mu \left(5/3 - \gamma \right). \tag{11}$$

In a laminar flow (first application of QGD equations mentioned in section 1), the averaging parameter τ is related to viscosity by $\mu = \tau\ p\,\mathrm{Sc}$, where Sc is the Schmidt number $\mathrm{Sc} = 5/(7 - \omega)$. In the present application, it accounts for subgrid dissipation and is taken as

$$\tau = \beta h / c_s \tag{12}$$

where the sound velocity $c_s = (\gamma R T)^{1/2}$ is estimated locally, h is the grid resolution and β is an empirical coefficient $0 \le \beta \le 1$. Its exact value is adjusted in each particular calculation.

2.3 Application to the given problem

The computational domain is represented in Figs.2a and 2b, corresponding to sections $z = 0$ and $y = 0$, respectively. Domain 1 has been considered in [1, 2]. The upper boundary ($z = 0$ in Fig. 2b) is the vehicle wall ahead of the engine inlet. The shape of the domain is adapted to the presence of an oblique shock wave ABC (dashed line) that originates from nose A. The nose of the body is located in the plane $x = 0$.

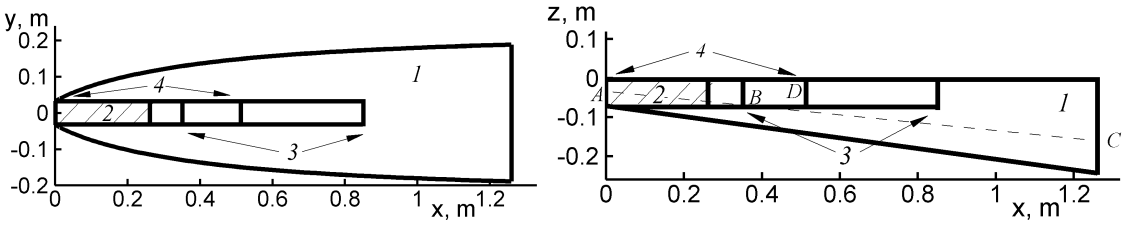

(a) **(b)**

Figure 2: Computational domain. (a) top view, (b) side view.

In the present work, we use a uniform rectangular grid with cubic cells. The absence of anisotropy in uniform grids makes them well-adapted to vortical configurations. We consider only a limited part of domain 1, namely the rectangular domains 2, 3 and 4.

Let us briefly comment upon the peculiarities of results obtained in the different domains.

In domain 3, whose left boundary is located somewhat downstream the nose, no oscillations were found. This is because oscillations originate from the nose (point A), outside of the domain. Actually the linear stability analysis [1, 2] revealed a very strong crossflow instability at the nose, turning progressively to more stable Mack's oblique first modes.

Domain 4 is such that the oblique shock crosses the lower boundary at point B. It reflects on that boundary and affects the flow further downstream, inducing oscillations that would not take place in the absence of artificial shock reflection.

Domain 2 (hachured in Fig. 2) is free from the above drawbacks and the corresponding results will be presented here. However, this domain is small compared with domain 1 and the simulation allows studying only the initial part of the turbulent flow. A better simulation would require a non-uniform grid that coarsens in the downstream direction and covers domain 1. Nevertheless results on domain 2 present some interest.

Domain 2 is a rectangular one $0 \le x \le 0.262,\ -0.033 \le y \le 0.033,\ \ -0.066 \le z \le -0.008$. Here and below lengths are expressed in meters. The upper boundary $z = -0.008$ corresponds to the wall.

We use a uniform space discretization $h_x = h_y = h_z = 0.001$ (further denoted as h). The time step is determined by the Courant condition. We write the latter as $h_t = \alpha h / c_0$, where α is the Courant number, $c_0 = (\gamma R T_0)^{1/2} = 299$ m/s and T_0 are the freestream sound velocity and temperature, respectively. It was found that convergence required $\alpha = 0.075$, resulting in $h_t = 2.5 \times 10^{-7}$ s. The number of time steps is not known a priori. It must be sufficiently large for oscillations to be observed. The coefficient that determines additional dissipation in Eq.(12) is taken as $\beta = 0.08$.

The discretized flow parameters are determined at the grid points. The values at the boundaries of the domain are determined as the half-sum of the values at the extreme and adjacent points. This form of boundary condition is a second-order space approximation [4]. The derivatives in Eqs.(2)-(8) at internal points are approximated by central differences. The time derivatives are approximated by first-order upwind scheme. Thus the numerical finite-difference algorithm is explicit-in-time, with a centered second-order approximation for all space derivatives.

The initial and boundary conditions are taken from the results of laminar steady flow over the whole vehicle according to the original Fluent flowfield calculations [1, 2].

As initial conditions we take the distribution of flow parameters (density, velocity components and pressure) in sections $x = 0.0015, 0.0615, 0.1215, 0.1815, 0.2415$ and $z = 0.066$. Using a linear space interpolation, we obtain the initial distribution in the whole domain.

The boundary conditions are set as follows.

- Along upstream boundary $x = 0$, we maintain constant values of ρ, u_x, u_y, u_z, p. As the boundary is located between the grid points, we need to maintain a constant half-sum of flow parameters at the extreme and adjacent points. The same method is used along the other boundaries.
- The boundary $z = -0.008$ corresponds to the vehicle wall. It is considered as adiabatic and characterized by $u_x = 0$, $u_y = 0$, $u_z = 0$, $\partial p / \partial n = 0$. The latter condition is specific to QGD equations and results from the no-flow condition through the wall [4, 5]. The condition $\partial \rho / \partial n = 0$ results from the adiabatic wall condition $\partial T / \partial n = 0$.
- The vehicle flies under an angle-of-attack equal to 4 degrees. The flow along the lower boundary $z = -0.066$ is oriented into the computational domain. Therefore we prescribe constant flow parameters along this boundary in the same way as for the upstream boundary.

- Along other boundaries we use *soft conditions*: $\partial\rho / \partial n = 0, \partial u_x / \partial n = 0, \partial u_y / \partial n = 0, \partial u_z / \partial n = 0, \partial p / \partial n = 0$, which is justified by the supersonic nature of the flow. However the same conditions were prescribed also in the subsonic zone near the wall.

Computations were carried out on highly-parallel computers K-100 and BlueGene/P of the Russian Academy of Science [9]. A parallel variant of the numerical algorithm was developed based on a decomposition of the computational domain by planes x = cste. The MPI standard was used to allow portability between computer systems. For the problem under consideration, parallelization results in a linear efficiency increase with increasing the number of nodes. However computer K-100 is approximately 10 times more efficient than BlueGene/P for an identical number of active nodes. The results presented here have been obtained using computer K-100 with 32 processor nodes. They requires approximately 12 hours of computing time ("wall time").

3 Results of numerical simulation

Isolines of density (a, b), temperature (c), pressure (d) and Mach number (e) have been plotted in Fig. 3 for section $x = 0.25$ as well as the projection of streamlines on the section plane. They exhibit the saddle point described by A. Ferri.

Density levels at times t = 0.01 s and t = 0.014 s are plotted in Figs 3a and 3b, respectively. The time evolution of vortical structure is visible in Figs3a and 3b.

Figures 3c to 3e are similar to Fig. 3b and present the isolines for temperature, pressure and local Mach number at t = 0.014 s.

Figure 4 is similar to Fig. 3 and presents flow parameters at the same time t = 0.014 s in section z = -0.0115. This section passes through the point marked with a black cross in Fig. 3.

Figure 5 is similar to Fig. 4 presents flow parameters at t = 0.014 s in section y = -0.001 that passes also through the point marked with a black cross in Fig. 3.

The isolevels are identical for Figs 3 to 5.

Studying oscillating processes in an unsteady flow requires considering the time evolution of some flow parameter. In Fig. 6 is plotted the time evolution of velocity component u_y at location $x = 0.25,\ y = -0.001,\ z = -0.0115$ (point marked with a black cross in Fig. 3). In Fig. 6a the time evolution of u_y is plotted over the whole computed time interval, from $t = 0$ to $t = 0.014$ s. The transition process begins at approximately t = 0.005 s, after a transient process for QGD to adapt to the NS initial field. Then the flow exhibits a typically turbulent character.

The same evolution is plotted in Fig. 6b with a dilated scale: from $t = 0.0125$ to $t = 0.014$ s. When transition begins, u_y is approximately equal to 5 m/s. When oscillations are established, their amplitude is approximately 50 m/s.

The calculation was repeated with a grid refined by a factor of 2 in all directions. The flow pattern was similar to the one plotted in Figs 3-5. However, due to available computational resources, the calculation could not be continued up to the time of established turbulence.

Let us consider the oscillation spectrum of u_y.

The frequency spectrum is calculated after completion of the transition process, i.e. from $t_0 = 0.005$ s. The time interval over which the spectral development is carried out is $T_0 = d_t\ (M_t - 1)$. The number of time points M_t must be even. We take $M_t = 3600,\quad T_0 = 0.0089975$ s.

The frequency dependence of E_k is plotted in Figs. 7a and 7b in logarithmic and linear scales, respectively. The oscillations of u_y exhibit four characteristic frequencies: 7.4, 12.8, 20 and 38 kHz. This is consistent with the conclusions of [1, 2] whose authors stated that the highest development rate for oscillations occurred at frequencies of the order of 10 kHz. Once turbulence has occurred, a broadband spectrum is set up, in which the signature of initial waves is combined with higher harmonics.

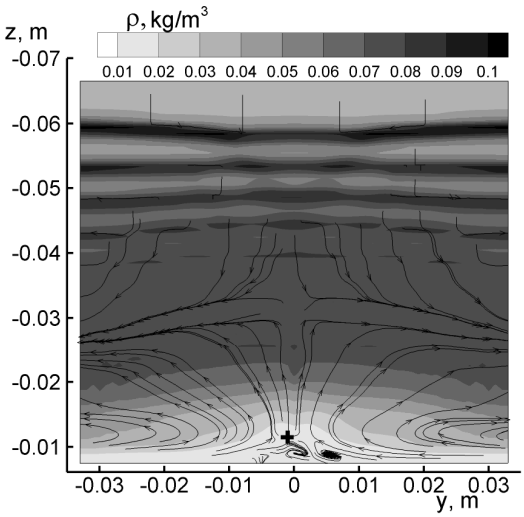

(a) density t = 0.01 s

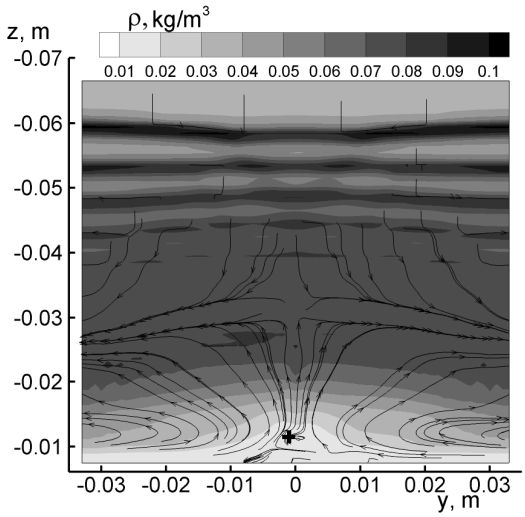

(b) density, t = 0.014 s

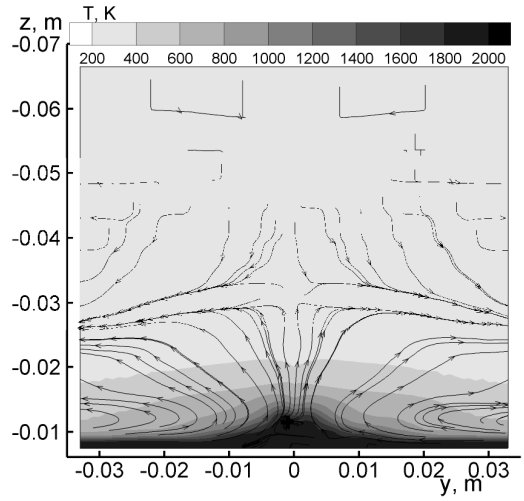

c) temperature, t = 0.014 s

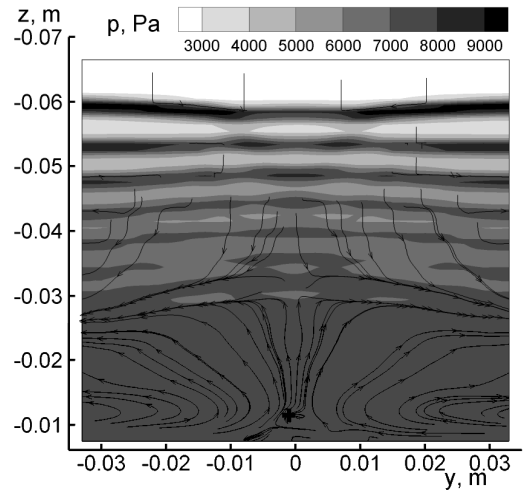

(d) pressure, t = 0.014 s

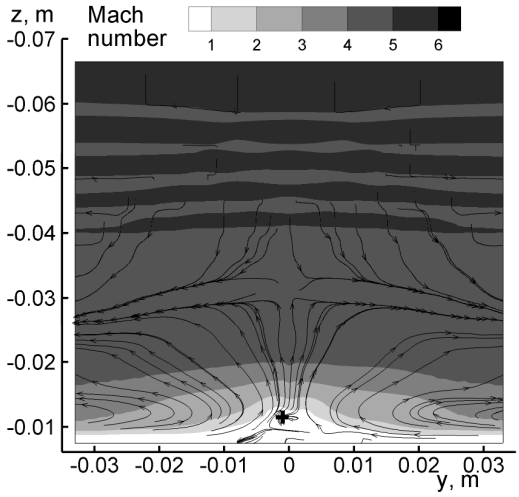

(e) Mach number, t = 0.014 s

Figure 3: Distribution of flow parameters at $x = 0.25$ m.

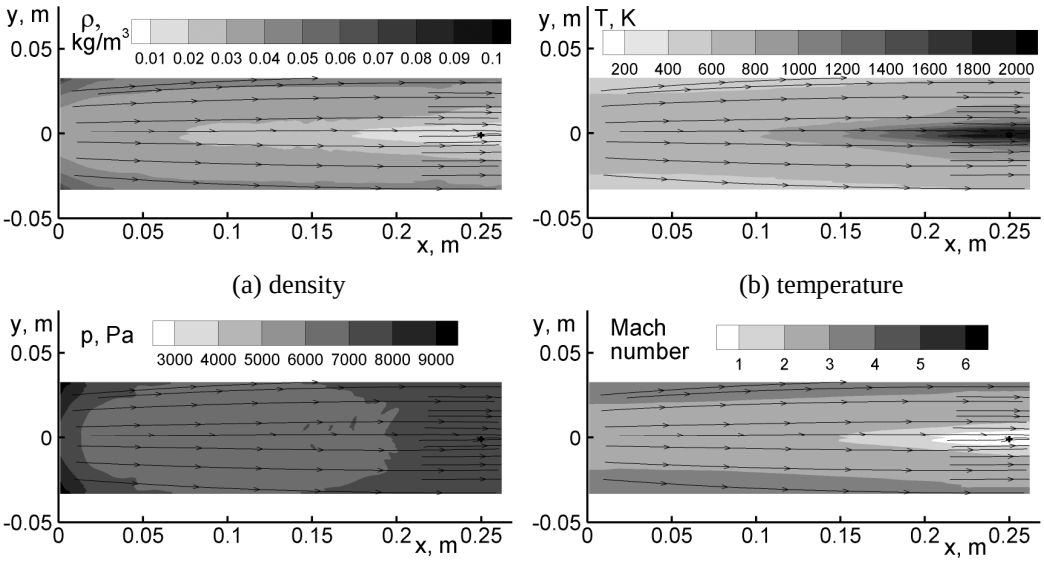

(a) density (b) temperature

(c) pressure (d) Mach number

Figure 4: Distribution of flow parameters at time t = 0.014 s in section z = -0.0115 m.

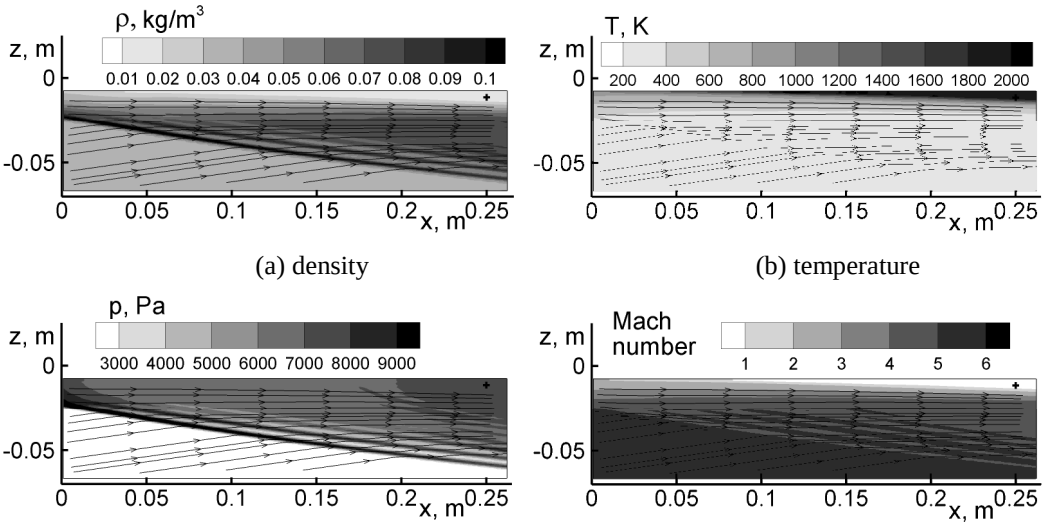

(a) density (b) temperature

(c) pressure (d) Mach number

Figure 5: Distribution of flow parameters at time t = 0.014 s in section y = -0.001 m.

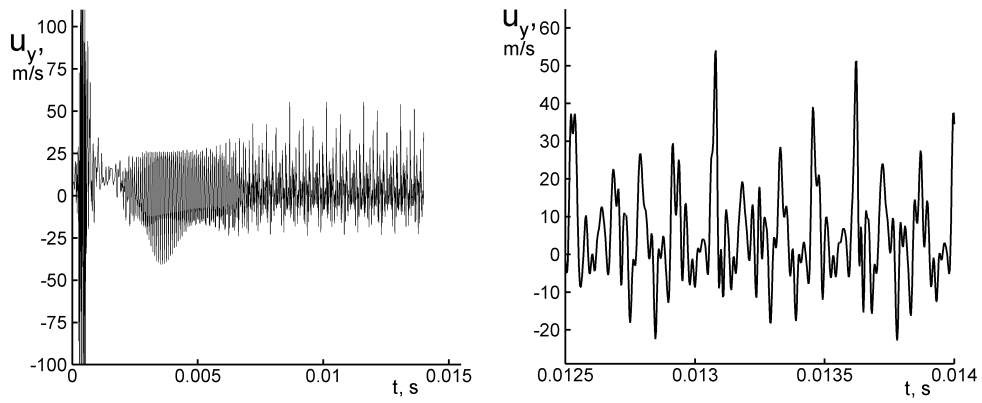

(a) (b)

Figure 6: Time evolution of velocity component u_y at location $x = 0.25$ m, $y = -0.001$ m, $z = -0.0115$ m .

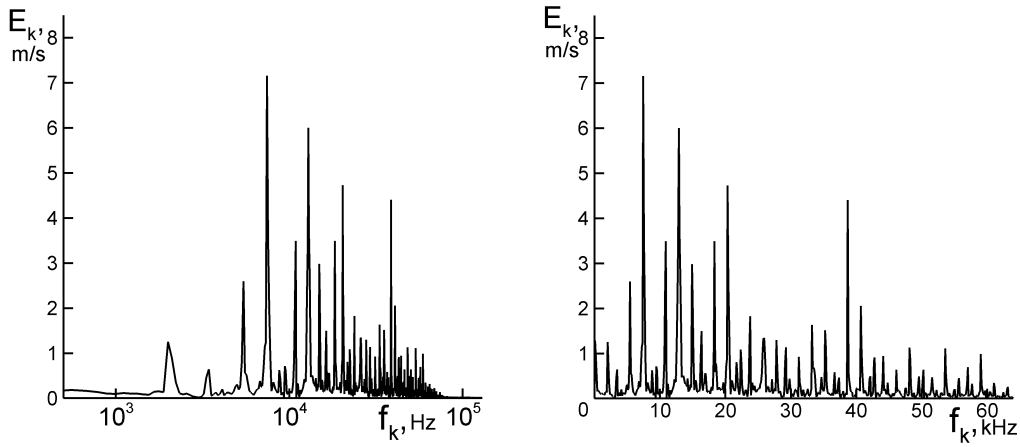

(a) (b)

Figure 7: Fluctuation spectrum of u_y at location $x = 0.25$ m, $y = -0.001$ m, $z = -0.0115$ m .

4 Conclusion

The present numerical work is based on Quasi-Gas Dynamics (QGD) equations. These equations reproduce a non-stationary flow in the region of laminar-turbulent transition close to the forebody of a hypersonic vehicle even for stationary conditions in the incoming flow. The fluctuations of velocity and other gas dynamic parameters have a stochastic character, whose limitations are associated with the time and space resolution of the calculation.
Although the computational domain is small and does not include the whole flowfield of interest, the main frequencies of the calculated fluctuations are consistent with data obtained by a linear stability analysis of the steady flow computed around the vehicle. More detailed information could be obtained using a more refined space grid and using a special metrics that would allow extending the computational domain over the whole forebody.

This work was partly supported by grant RFFI 10-01-00136.

References

[1] Orlik E., Kornilov V., Ferrier M., Fedioun I. and Davidenko D. 2009. Hypersonic laminar/turbulent transition: computation and experiments. In: *3rd EUCASS Conf.*, Proc. on CD-ROM.
[2] Ferrier M., Fedioun I., Orlik E. and Davidenko D. 2009: Modal Linear Stability of the Near-Wall Flow on a Hypersonic Forebody, *J. of Spacecraft and Rockets*, 46: 51-66.
[3] Chetverushkin B.N. 2004. Kinetic Schemes and Quasi-Gasdynamic System of Equations, MAKS, Moscow.
[4] Elizarova T.G. 2009. Quasi-Gas Dynamic Equations. Springer, IBSN 978-3-642-00291-5.
[5] Sheretov Yu.V. 2009. Dynamics of continuous media with time-space averaging. Moscow-Izhevsk, NITs *Regular and Chaotic dynamics.* (in Russian)
[6] Antonov A.N., Elizarova T.G., Chetverushkin B.N. and Sheretov Yu.V. 1990. Numerical modeling of pulsating regimes accompanying the supersonic flow around a hollow cylinder. *J. Computational Mathematics and Mathematical Physics*, 13:139-144.
[7] Elizarova T.G., Nikolskii P.N. and Lengrand J.C. 2008. A new variant of subgrid dissipation for LES method and simulation of laminar-turbulent transition in subsonic gas flows. In *Advances in hybrid RANS-LES Modelling*, Springer, pp. 289-298.
[8] Elizarova T.G. and Seregin V.V. 2009. Filtered simulation method for turbulent heat and mass transfer in gas dynamic flows. In *Proceedings of the 6-th International Symposium on turbulence, heat and mass transfer*, Rome, Italy, 14-18 September 2009. Ed. K. Hanjalie, Y. Nagano, S. Jakirilic. Begell House Inc., pp.383-386.
[9] http://www.kiam.ru, http://hpc.cs.msu.ru.